AIAA JOURNAL
Vol. 46, No. 2, February 2008

Further Refinement and Validation of Material Models for Hypervelocity Gouging Impacts

J. D. Cinnamon,* A. N. Palazotto,† and A. G. Szmerekovsky‡
Air Force Institute of Technology, Wright–Patterson Air Force Base, Ohio, 45433

DOI: 10.2514/1.25035

The gouging impact phenomenon which occurs at the Holloman Air Force Base High-Speed Test Track during hypervelocity impact testing is examined further. The material constitutive models for VascoMax 300 and 1080 steel are refined, and extended into the high-strain-rate regime, using results from flyer plate impact experiments. These experiments are simulated using the hydrocode CTH to improve the material strength models at high strain rates. The improved viscoplastic models are then validated by comparing laboratory hypervelocity impact tests to CTH simulations. The final material models are then used in sled/rail impact simulations for the Holloman Air Force Base High-Speed Test Track gouging problem. These full-sled simulations match previous experimental findings extremely well.

I. Introduction

THE Holloman High-Speed Test Track (HHSTT) is a U.S. Air Force test facility which conducts hypervelocity impact testing. The HHSTT performs this testing using rocket-propelled sleds that ride on a 15.5 km steel rail track. The rocket sleds are held on the rails by steel "shoes/slippers." Fig. 1a illustrates the sled and shoe geometry. Current testing capability allows for impact testing in the 1–2 km/s range, with near-term goals of a velocity greater than 3 km/s. At these velocities, the shoes impact the rail due to the motion experienced by the test sled. The severity of the impact varies, but in certain cases can result in catastrophic failure of the test sled. Inspections of the rails after test events have revealed damage in the form of gouges [1]. Gouges associated with high-energy impacts are characterized by a teardrop-shaped shallow depression in the material (see Fig. 1b). These gouges typically are the result of a high-pressure core developing at the material interface and high-viscoplasticity that leads to material mixing (i.e., shoe material becoming embedded within the rail, and vice versa) [1–6].

Simulations of the hypervelocity gouging process have previously been conducted [2–6] using the hydrocode CTH [7,8]. A plane-strain model of the shoe/rail interaction was developed as an accurate, and computationally necessary, representation of the actual impact geometry [2–6]. These previous models were limited by the material constitutive relationships present within the CTH code. Therefore, an effort was undertaken to perform experimentation on the specific materials (VascoMax 300 for the shoes, 1080 steel for the rails) to arrive at accurate constitutive models [9,10]. These previous efforts were limited to Split Hopkinson Bar and Taylor Impact tests, with strain rates in the 10^3/s range. The material flow models developed accurately simulated both of these experimental tests [10–12]. However, the high-energy impact environment typically generates strain rates well in excess of those levels.

Therefore, in this work, flyer plate experiments are conducted to extend the material constitutive behavior into the 10^4–10^5/s strain-rate regime. The CTH code is used to deduce new flow models that are capable of matching the measured stress waves in the flyer plates. These new models are then used within CTH to simulate laboratory hypervelocity gouging experiments previously conducted.

With these new validated material constitutive models, the sled/rail gouging phenomenon is accurately modeled within the CTH code and preliminary observations are made regarding the conditions which lead to gouging. The results of these simulations match experimentally observed gouge characteristics well.

II. High-Energy Material Deformation

The typical fashion in which material deformation is considered within computational codes is through constitutive models. In dynamic deformation, a simple description of the yield stress is insufficient. More complex material models are necessary, which modify the flow stress σ by accounting for variations in strain, strain rates, and temperature. One of the most widely used constitutive models is the Johnson–Cook model [13].

$$\sigma = [A + B\varepsilon^n][1 + C\,\ell n\,\dot{\varepsilon}^*][1 - T^{*m}] \tag{1}$$

where ε is the equivalent plastic strain, $\dot{\varepsilon}^* = \dot{\varepsilon}/\dot{\varepsilon}_0$ is the dimensionless plastic strain rate for $\dot{\varepsilon}_0 = 1.0\ \mathrm{s}^{-1}$, and T^* is the homologous temperature defined as

$$T^* = (T - T_{\mathrm{room}})/(T_{\mathrm{melt}} - T_{\mathrm{room}}) \tag{2}$$

The constants A, B, C, m, and n are determined via experimental testing and empirically curve-fitting the model to the results. In a similar vein, another widely used constitutive model is the Zerilli–Armstrong model [14].

$$\sigma = A + (c_1 + c_2\sqrt{\varepsilon})e^{(-c_3T + c_4T\,\ell n\,\dot{\varepsilon})} + c_5\varepsilon^n \tag{3}$$

where $\dot{\varepsilon}$ is the equivalent plastic strain rate, and A, c_1, c_2, c_3, c_4, c_5, and n are experimentally determined constants. The Zerilli–Armstrong is a more materials science oriented approach. For instance, $c_1 = 0$ for a face centered cubic material lattice, whereas $c_2 = 0$ for a body centered cubic lattice. The Johnson–Cook model is purely empirically based. The variation in form provided by the Zerilli–Armstrong model adds capability to alter the constitutive relationship (which will become important later in this work).

The determination of the experimental constants for either of these models comes from uniaxial tests, such as simple quasi-static tests and Split Hopkinson Bar (SHB) tests. These relatively simple tests can provide information on stress and strain at given temperatures for strain rates in the 10^3/s range. However, the high-energy impacts at

Presented as Paper 2086 at the 47th AIAA/ASME/ASCE/AHS/ASC Structures, Structural Dynamics, and Materials Conference, Newport, RI, 1–5 May 2006; received 8 May 2006; revision received 5 December 2006; accepted for publication 7 December 2006.

*Lieutenant Colonel, United States Air Force, Ph.D., Professional Engineer, Adjunct Assistant Professor, Department of Aeronautics and Astronautics. AIAA Member.

†Professor, Department of Aeronautics and Astronautics. AIAA Fellow.

‡Lieutenant Colonel, United States Air Force, Ph.D., Assistant Professor, Department of Engineering Mechanics, United States Air Force Academy. AIAA Member.

a) HHSTT sled/shoe geometry **b) Shoe/rail section with gouge**

Fig. 1 Holloman high-speed test track: a) sled/shoe geometry, and b) shoe/rail section with gouge.

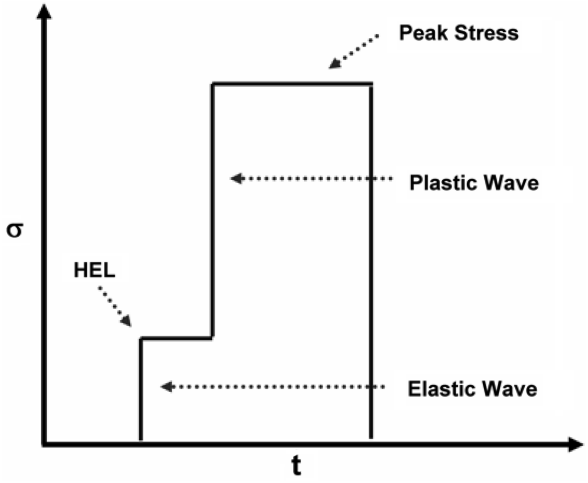

Fig. 2 Idealized stress vs time plot for a uniaxial planar impact.

the HHSTT generate material strain rates on the order of 10^5–10^6/s [4–6].

To generate data to extend previously developed flow models [9–12], a higher strain-rate uniaxial test is required. The type of test that is typically employed is the flyer plate impact experiment [15]. These high-velocity impact tests can provide stress measurements with respect to time for a given impact [16]. The resulting stress-time curves are characterized by an elastic precursor wave, followed by the plastic deformation wave, as illustrated in Fig. 2. The magnitude of the elastic precursor wave is known as the Hugoniot elastic limit (HEL). This value provides one of the accepted estimates for the dynamic yield (flow) stress of the material, which is often taken as a material constant. The flyer plate experiments can be performed in such a manner as to yield both the HEL and the peak stresses at given impact velocities.

These flyer plate experiments provide unique information in the formulation of a material constitutive model. The Johnson–Cook or Zerilli–Armstrong models serve to establish the magnitude of the HEL, whereas the material equation of state (EOS) governs the material behavior at the stresses experienced in the plastic deformation wave. Therefore, these experiments require a one-dimensional uniaxial strain code simulation of the impact conditions, with the capability to adjust the material constitutive models and the equation of state. Both of these elements could be adjusted to refine the material models to match the experimental results.

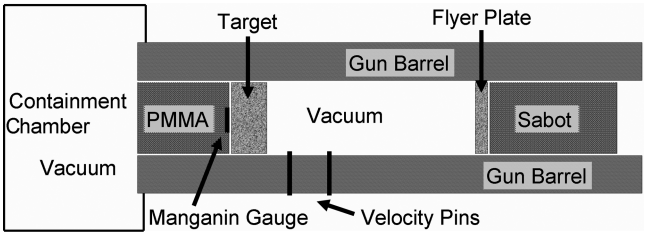

Fig. 3 Schematic of flyer plate experimental tests 7-1878 and 7-1879.

III. Flyer Plate Impact Experiments and Constitutive Model Development

To extend the previously determined material models for VascoMax 300 and 1080 steel to the higher strain-rate regime, a series of flyer plate experiments was conducted. The tests were conducted at the Impact Physics Laboratory of the University of Dayton Research Institute (see Acknowledgments). One of the two test configurations appears in Fig. 3. These two tests (one each for the specific materials) were conducted with the goal of recording the HEL. The flyer plate (3 mm thickness) was shot against a 6-mm-thick target of the same material, with a manganin stress gauge attached to the back of the plate, held by 12 mm of polymethyl methacrylate (PMMA). Two additional experiments were conducted for each material in the second test configuration. For these tests, the target was composed of 2 mm of material, a stress gauge, and 12 mm of additional material. These shots were performed to record the stress wave within the material as it passes. This geometry was not suitable for the detection of the HEL because of insufficient resolution. Table 1 summarizes the preceding test conditions.

The stress gauge measurements were taken for each of the cases, as well as velocity information from the velocity pins. The hydrocode CTH was chosen to simulate these impacts through a one-dimensional model. Because CTH will be used in hypervelocity impact simulations, using this particular code and its EOS formulation was essential to building an accurate constitutive model.

Tests 7-1878 and 7-1879 were simulated first. The modification of the constitutive model affected the magnitude of the HEL prediction, as well as the peak stress. Although the EOS dominated the solution, up to a 10% modification could be made to the peak stress by allowing for higher strengths at strain rates of 10^5/s (which is the level computed by CTH as the strain rate of the flyer plate tests). As expected, these modifications to the constitutive model were necessary to make the HEL prediction match the flyer plate experiments. The previous models, developed from the SHB tests,

Table 1 Summary of flyer plate tests

Test	Flyer	Velocity, m/s	Target
7-1874	3 mm VascoMax 300	685	2 mm + gauge + 12 mm VascoMax 300
7-1875	3 mm 1080 steel	669	2 mm + gauge + 12 mm 1080 steel
7-1876	3 mm VascoMax 300	450	2 mm + gauge + 12 mm VascoMax 300
7-1877	3 mm 1080 steel	437	2 mm + gauge + 12 mm 1080 steel
7-1878	3 mm VascoMax 300	891	6 mm VascoMax 300 + gauge + 12 mm PMMA
7-1879	3 mm 1080 steel	891	6 mm 1080 steel + gauge + 12 mm PMMA

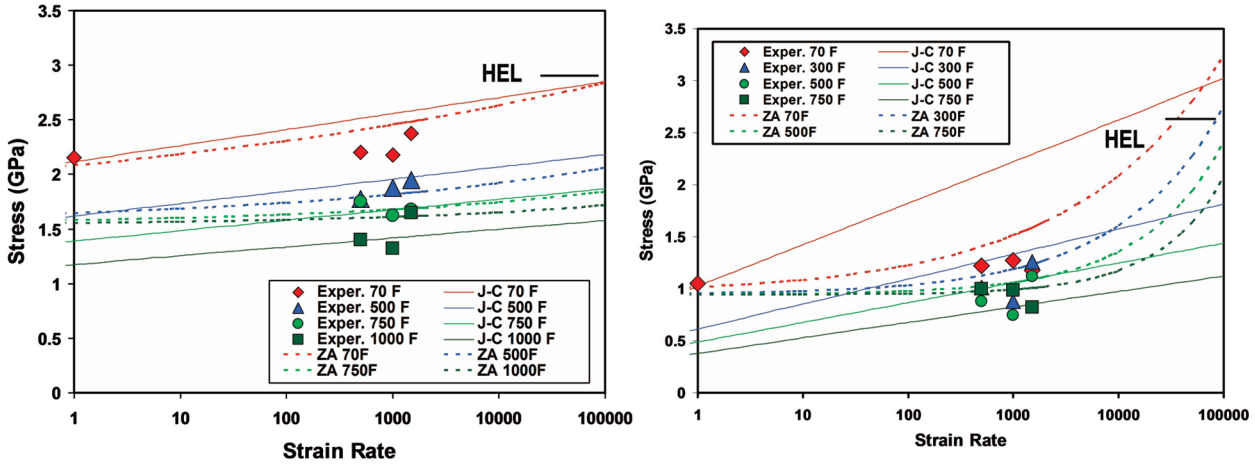

a) b)

Fig. 4 Models required to match flyer plate data and also match SHB data as much as possible: a) stress vs strain rate, VascoMax 300, 1% strain, and b) stress vs strain-rate, 1080 steel, 6% strain.

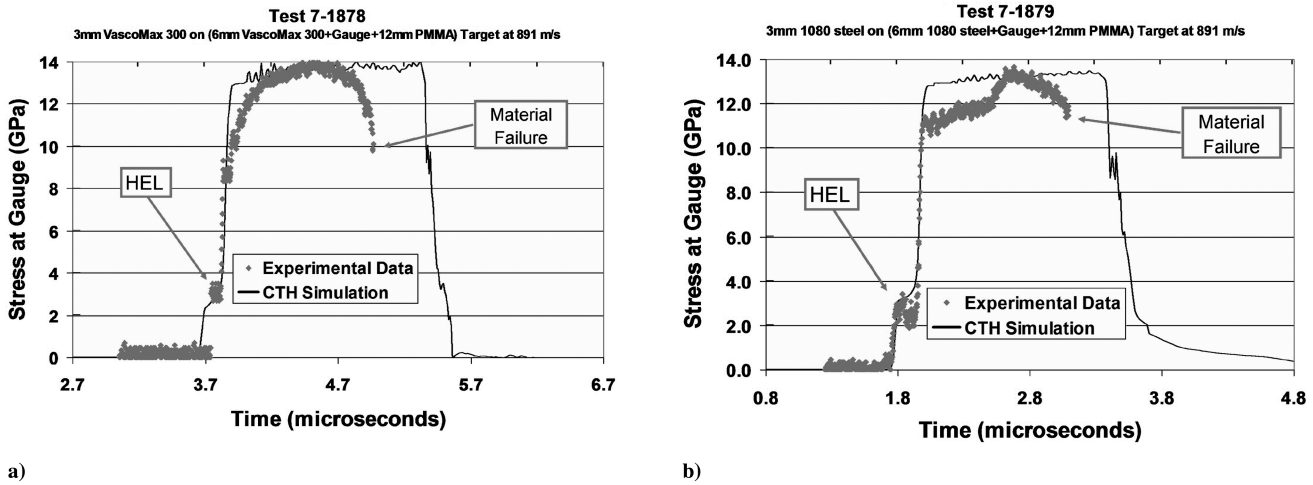

a) b)

Fig. 5 Shock stresses as a function of time for the Johnson–Cook model: a) VascoMax 300, and b) 1080 steel.

were underpredicting the flow stress at the strain-rate levels experienced in the flyer plate impacts. By requiring these adjustments, the flyer plate experiments were effectively bridging the gap between the lower strain-rate SHB tests, and the very high strain-rate impacts dominated by the EOS calculations.

An iteration process was undertaken by the authors to adjust the parameters of the Johnson–Cook and Zerilli–Armstrong models to find a best match between the CTH simulations and the experimental flyer plate tests. That is, the constants of these models were adjusted, then the CTH code was used to simulate the flyer plate tests, and a comparison was made between the measured stress and the CTH predicted stress. The model constants were iterated to create a "best-fit" match for all three tests available for each material. Initially, it appeared as if the Johnson–Cook model (which had been employed to date by the authors) might continue to be sufficient as the constitutive model for these materials. However, because of the linear relationship between effective stress and strain rate, the higher stress estimates for $10^5/\mathrm{s}$ strain rate required to match the flyer plate tests made the model overestimate the SHB regime data. Because of this, the greater flexibility of the Zerilli–Armstrong model became important. It was possible to construct a Zerilli–Armstrong model that came close to matching the SHB data, and still made the fit to the flyer plate data possible. Figure 4 illustrates the Johnson–Cook (JC) and Zerilli–Armstrong (ZA) models that were required to match the flyer plate data and also match the SHB data (Exper.) as much as possible. Note that the HEL derived from flyer plate experiments (discussed next) appears also. It is clear that the Zerilli–Armstrong formulation is superior in its ability to maintain better matches to both sets of experimental data.

Figure 5 illustrates the CTH simulation of the shock stresses as a function of time for the Johnson–Cook model developed to match all the flyer plate experiments. Figure 6 is the same simulation, using the Zerilli–Armstrong model. On both figures, the experimental stress gauge data are depicted on the simulation. In addition, where the gauge or material failed during the experiment, that fact is annotated on the figure. Table 2 summarizes the constants for both models which were determined to match the flyer plate stress data. Because of the better fit to the SHB data, the Zerilli–Armstrong model was chosen as the one with which to continue the investigation.

Figure 7 illustrates the fit that the Zerilli–Armstrong model and the EOS in CTH are able to make to the remaining experimental flyer plate tests (which were performed in the second configuration). The stress wave was measured within the material, as opposed to at the rear of the target. Additionally, these tests were conducted at a lower velocity to provide varying peak stresses to match the models against.

Based on the results, the authors conclude that a very accurate constitutive model has been developed which creates a close match to the flyer plate impact test data and the previously performed SHB tests. Although the JC model developed from the flyer plate experiments tended to produce similarly good results to those appearing in Fig. 7, the poor fit to the SHB data was a concern. The authors returned to previously conducted analyses in which the SHB tests were simulated in a finite element code [12]. In that work, the

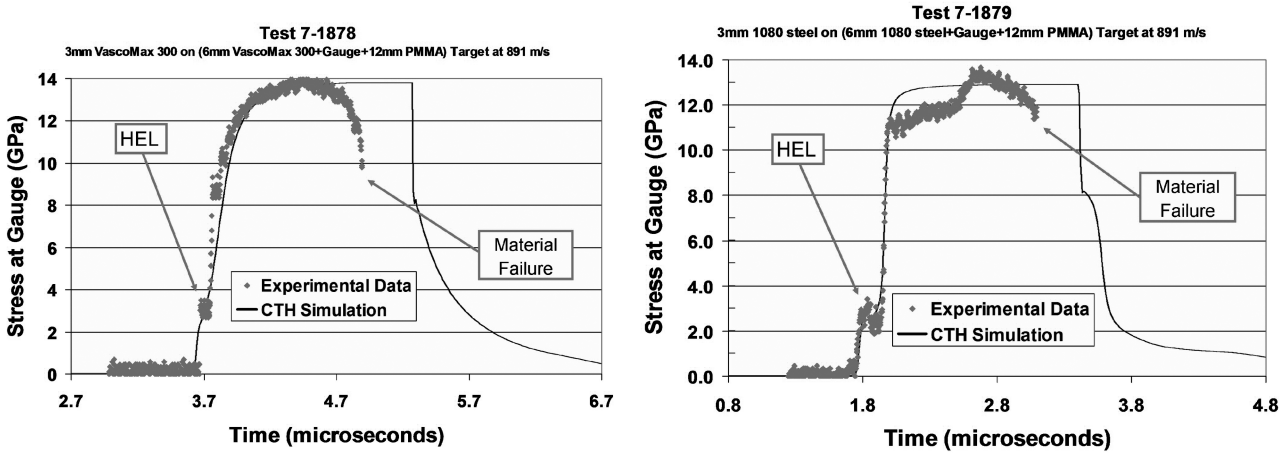

a) b)

Fig. 6 Shock stresses as a function of time for the Zerilli–Armstrong model: a) VascoMax 300, and b) 1080 steel.

posttest geometry of the SHB specimens was matched using the Johnson–Cook model which was developed before the flyer plate tests. Returning to those simulations, the new JC model developed in this paper failed to accurately replicate the observed posttest geometry. Figure 8 shows both the previous simulation for VascoMax 300 (which did match those posttest measurements) and the new simulations based on an adjusted JC model from the flyer plate data. The overestimated flow stress predictions for the intermediate strain rates (10^2–10^3/s) from this adjusted model leads to less necking than was observed experimentally. However, applying the Zerilli–Armstrong model, which more accurately reflects the intermediate strain-rate regime, would more closely match the correct geometry in the SHB simulations. This comparison, along with the better fit of the Zerilli–Armstrong model to the SHB data and the good results generated in the flyer plate test simulations, led the authors to choose the Zerilli–Armstrong model for all further simulations in CTH of these materials undergoing dynamic deformation (in this work and future applications).

IV. Validation of the Material Constitutive Models

To ensure these new Zerilli–Armstrong constitutive models were experimentally validated against all the experimental data available to the authors, simulations of previously conducted impact tests were conducted in CTH using these new models.

The first series of tests that were replicated was a Taylor Impact test conducted with VascoMax 300 and 1080 steel projectiles shot against a rigid target of VascoMax 300. In that previous investigation, the material constitutive models were based exclusively on the SHB data [10,11]. The authors reaccomplished the CTH simulations and found that these new models did not significantly alter the previously observed results. That is, these flow stress models were able to successfully match Taylor cylinder mushroom diameter, final specimen length, and undeformed section length within 5% of experimental values. This result is an expected one, as the strain rates for Taylor Impact tests are on the order of 10^3/s. That is, these impact tests reside in the same intermediate strain-rate neighborhood as the SHB tests.

Table 2 Model constants for VascoMax 300 and 1080 steel

Property	1080 steel	VascoMax 300
ZA: A, GPa	0.825	1.42
ZA: c_1, GPa	4.0	4.0
ZA: c_2, GPa	0	0
ZA: c_3, eV^{-1}	160.0	79.0
ZA: c_4, eV^{-1}	12.0	3.0
ZA: c_5, GPa	0.266	0.266
ZA: n	0.289	0.289
JC: A, GPa	0.7	2.1
JC: B, GPa	3.6	0.124
JC: C	0.17	0.03
JC: m	0.25	0.8
JC: n	0.6	0.3737

The next series of tests simulated was the laboratory hypervelocity gouging tests conducted by the authors to create a high-strain-rate event approximating the gouging phenomenon at the HHSTT [17,18]. Four test shots were conducted with sufficiently high-impact angles to ensure gouge generation. Additionally, two target types were shot: one rail with iron-oxide coating, and the other with epoxy coating. These are the two coatings in use on the rails at the HHSTT to mitigate the formation of gouging. Table 3 summarizes the test shots and the resulting gouges.

Figure 9 is a high-speed photograph of the impact event. The projectile entered the frame from the left, and had impacted the epoxy-coated rail surface. The flare generated indicates the large thermal input into the rail, which was previously reported [1,19,20]. Figure 10 shows two of the four gouges created in these hypervelocity gouge tests. The view is looking down on the gouges, with the velocity vector of the projectile left to right in the photographs.

To characterize these deformations as gouging, a similar procedure of metallurgical analysis was conducted on these laboratory gouges as was performed on a gouged rail from the HHSTT [19,20]. The gouges were cut along their length and examined through the depth into the rail material. In previous work, gouges exhibited characteristic microstructure changes, indicative of 1080 steel heating above the austenizing temperature of 725°C and then rapidly cooling. This large thermal event was identified as one of the key elements of a gouging impact. If this large thermal profile is a key element of gouging, we should expect CTH to generate those same thermal profiles as part of the material model validation process. Recall that these constitutive models are viscoplastic in nature, which establishes their incorporation of material temperature in their flow strength predictions.

Therefore, the gouges were sectioned and prepared for optical microscopy. Figure 11 illustrates the metallurgical examination of test he-1; the coating has been removed by the gouging impact. There is also a micrograph of an undamaged rail head section provided for comparison, on which the coating still appears. One can see the evidence of microstructural change similar to that reported for an examined gouge from the HHSTT [19,20]. From this investigation, it appears that the microstructure is changed down to approximately 1.0 mm. This indicates that the 1080 steel heated above the austenizing temperature and then cooled rapidly following the impact. The information that this provides for model validation is that we should expect to see temperatures of approximately 1000 K down to 1.0 mm into the rail during the gouging process.

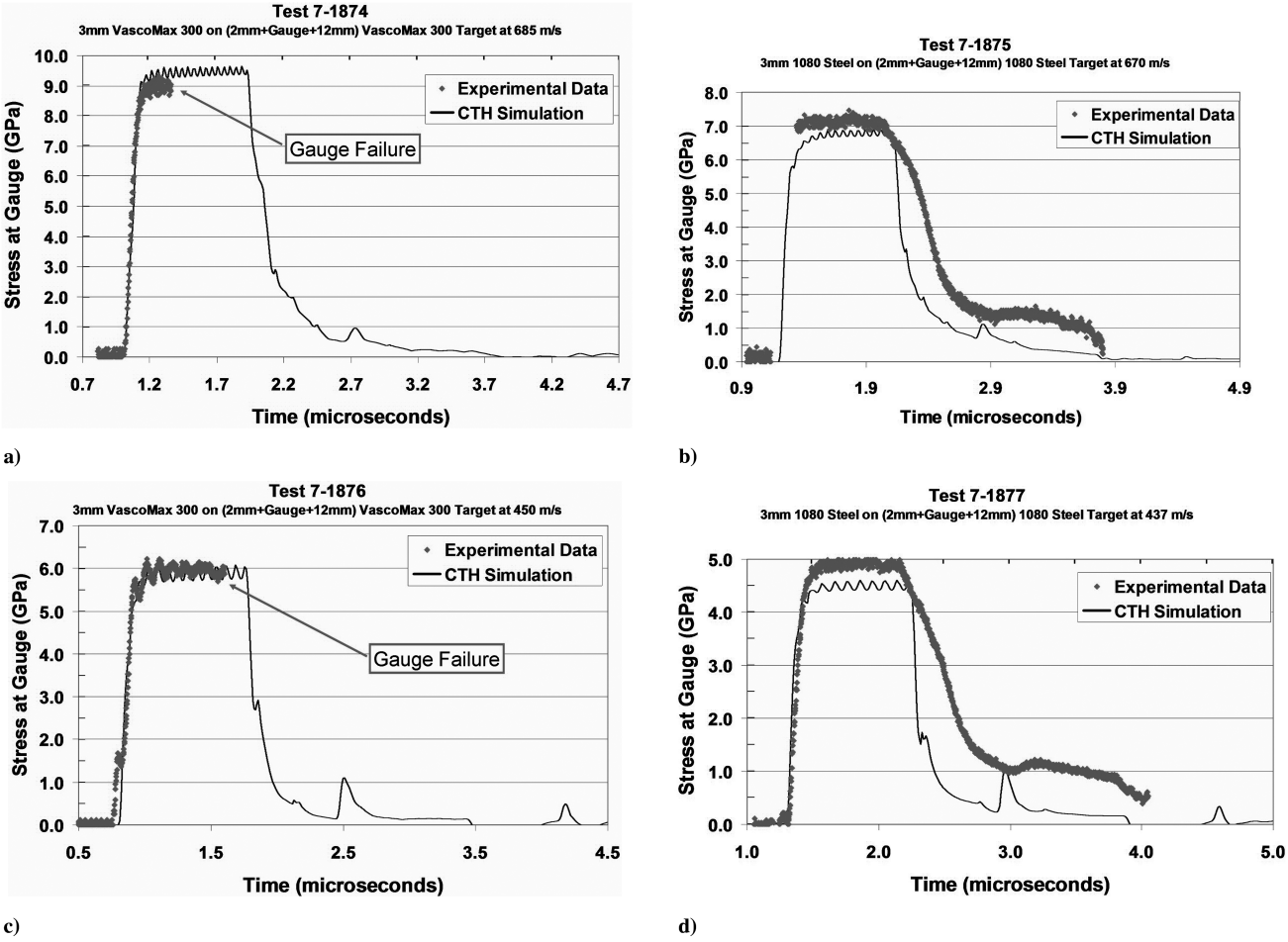

Fig. 7 Stress vs time for test a) 7-1874, VascoMax 300, b) 7-1875, 1080 steel, c) 7-1876, VascoMax 300, and d) 7-1877, 1080 steel.

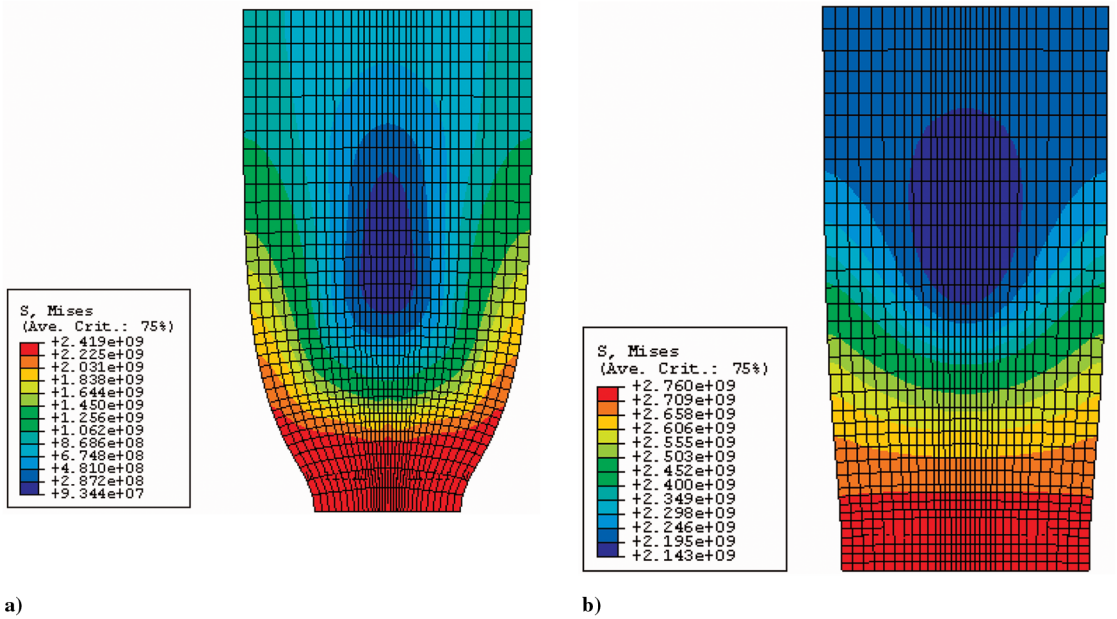

Fig. 8 Stress, Pa, SHB test for VascoMax 300 for a) previous JC model, and b) current JC model.

The four hypervelocity gouging impacts described in Table 3 were simulated in CTH with the Zerilli–Armstrong model constants delineated in Table 2. For the EOS model, CTH has an experimentally based EOS table for these materials developed by Sandia National Laboratories. A two-dimensional plane-strain model of the impacts was used. The suitability and accuracy of this approach was previously examined [17,21]. Using this approach, the cylinder with a hemispherical nose is modeled as a unit-thickness plate with a rounded leading edge. Figure 12 illustrates this model (with the velocity vector depicted). The high-speed photography available from the impacts indicated that the projectile oriented during flight in such a manner as to impact the target rail as depicted

Table 3 Laboratory hypervelocity gouge test results

Test	Coating	Angle, deg	Impact velocity, m/s	Gouge depth (measured), mm
hi-1	oxide	10	2225	0.5 ± 0.1
hi-2	oxide	15	2150	1.0 ± 0.1
he-1	epoxy	15	2147	1.0 ± 0.1
he-2	epoxy	10	2163	0.5 ± 0.1

in Fig. 12. Whereas the velocity vector was still oriented at 10 or 15 deg to the rail surface, the long axis of the projectile was aligned with the longitudinal axis of the target rail.

Figure 13 is of impact test he-1, with an impact velocity of 2147 m/s, and an impact angle of 15 deg. The solution of the impact scenario shows the characteristic material mixing and high plasticity of gouging. Additionally, Fig. 14 illustrates the pressure and strain rate associated with 10 μs. Note that the strain rates computed by CTH are predominately in the 10^4–10^6/s range in the gouging region. The four simulations of the laboratory gouging shots demonstrated excellent agreement to experimentally observed values for gouge depth. Table 4 summarizes these results.

The characteristics of hypervelocity gouging, such as a high pressure concentration [4–6] at the gouge location and material mixing, are evident in these simulations. Additionally, localized temperatures (illustrated in Fig. 15) were generated that could create the microstructural changes reported in the literature and are evident in Fig. 11 [19,20]. Note that an austenizing temperature of 1000 K is generated by CTH in Fig. 15 down to approximately 1.0 mm below the gouge depth. This matches the experimentally observed temperature profile in the gouge specimens. Therefore, the experimentally determined thermal profile from the metallurgical study validated the CTH simulation. Figure 16 illustrates this agreement.

The goal of these experiments and simulations was to validate the new material models for VascoMax 300 and 1080 steel for use in CTH. The hypervelocity gouging tests were as close, in a laboratory sense, as the authors could get to the conditions at the HHSTT. The plane-strain simulations show outstanding agreement to the experimental tests in terms of gouge depth. This success, as compared to earlier efforts, can be attributed to a new strength model that incorporates the experimental flyer plate data with strain-rates on the order of 10^5/s. Also, the metallurgically determined microstructural change resulting from the thermal aspect of the gouging event was replicated in the CTH simulation. The depth of the temperature change indicated in CTH closely matched the experimental findings.

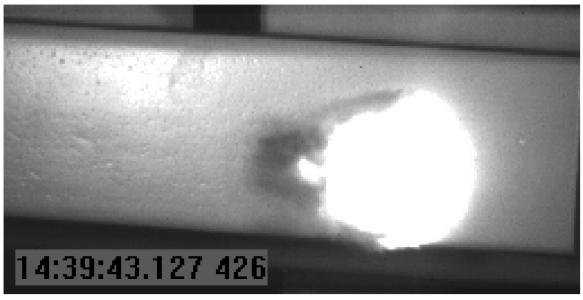

Fig. 9 High-speed photograph of hypervelocity impact on epoxy-coated rail.

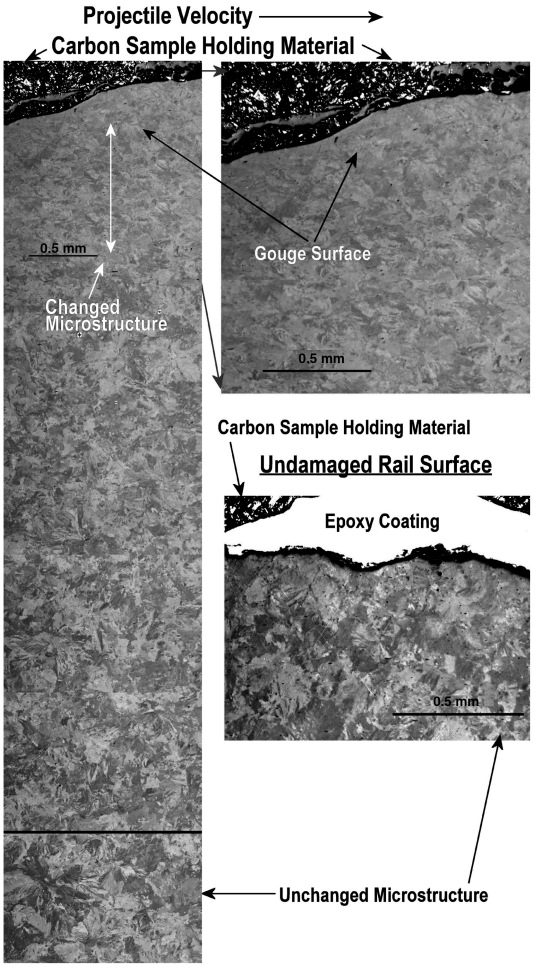

Fig. 11 Metallurgical examination of test he-1.

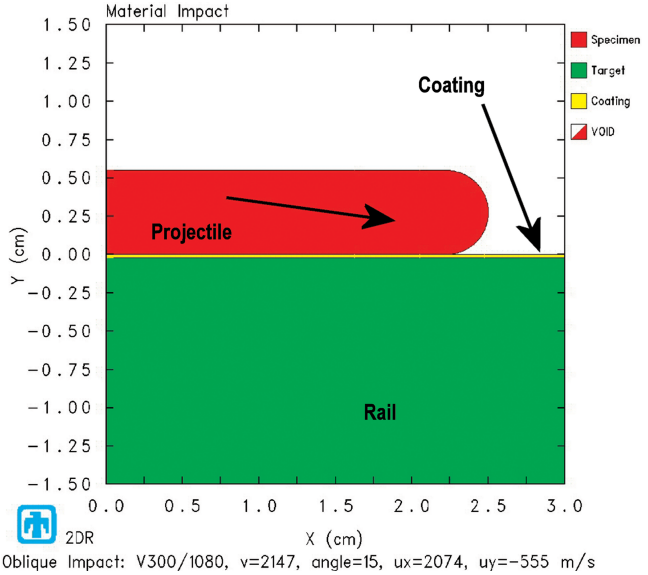

Fig. 12 CTH model of hypervelocity gouging test, with velocity vector depicted.

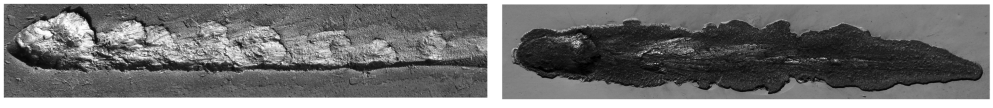

a) **b)**

Fig. 10 Comparison of two gouges created on a) iron-oxide-coated rail, and b) epoxy-coated rail.

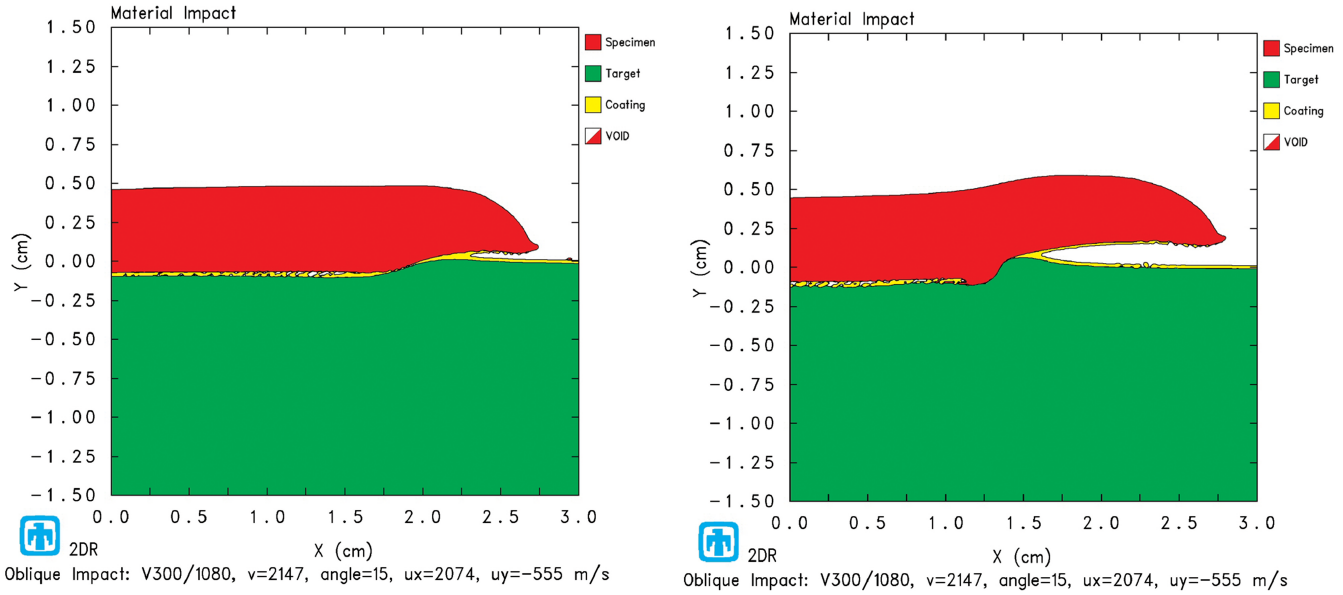

Fig. 13 Simulation of test he-1 at a) 5.0 μs, and b) 10 μs.

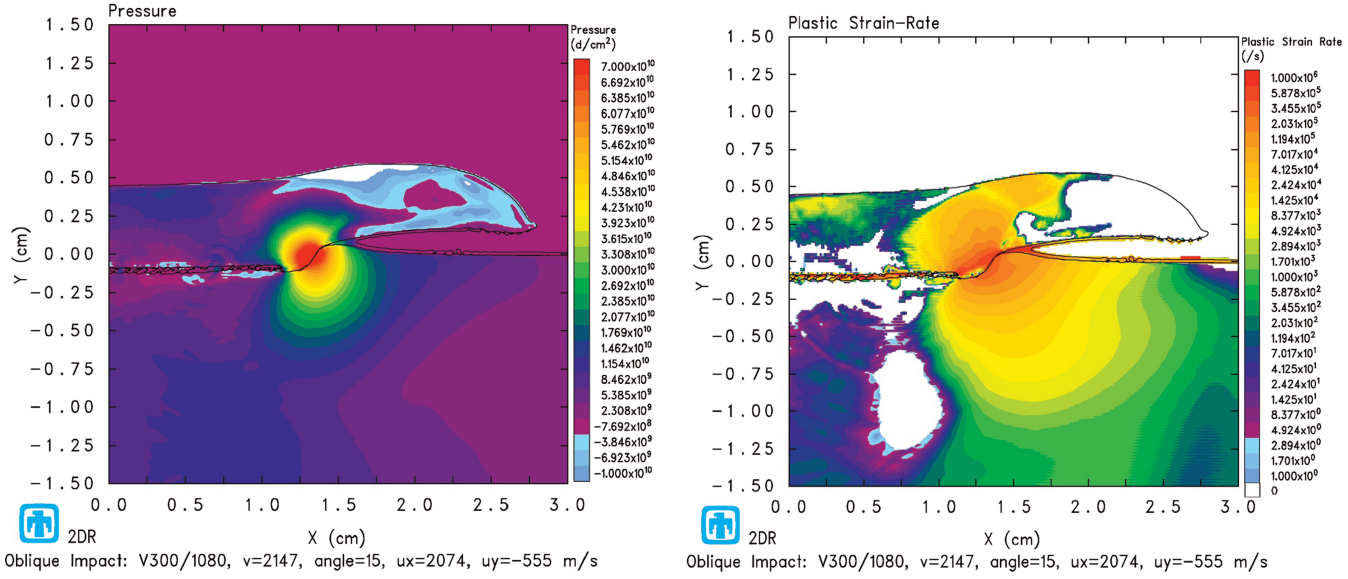

Fig. 14 Comparison of test he-1 at 10 μs for a) cell pressure, and b) strain rate.

V. CTH Modeling of HHSTT Gouge Scenario

With the validated Zerilli–Armstrong flow stress model, and the built-in EOS tables for these two materials, a CTH model can be used to simulate the HHSTT gouging scenario with high confidence in the accuracy of the material models. A full-scale model of the sled shoe/rail gouging problem was previously developed [4–6]. By modifying that previous effort with these validated material models, a further investigation was made into the gouging phenomenon. The model of the sled/rail interaction is also a two-dimensional plane-strain implementation, as illustrated in Fig. 17.

As previous investigators found, there are three primary mechanisms to replicate the gouging phenomenon in CTH. The first is providing the shoe with sufficient vertical impact velocity to deform the rail and initiate material mixing and gouging. In other words, a threshold vertical kinetic energy exists, beyond which gouging is created. Gouging includes aspects like material "jetting" and mixing, in which shoe material remains within the rail after impact and vice versa. Impacts that are simulated below this threshold energy cause a glancing impact that can be described as "scraping" or "wear." There is permanent material deformation and

Table 4 CTH gouge simulation comparison to experiment

Test	Coating	Angle, deg	Impact velocity, m/s	Gouge depth (measured), mm	Gouge depth (simulated), mm
hi-1	oxide	10	2225	0.5 ± 0.1	0.6
hi-2	oxide	15	2150	1.0 ± 0.1	1.1
he-1	epoxy	15	2147	1.0 ± 0.1	1.1
he-2	epoxy	10	2163	0.5 ± 0.1	0.5

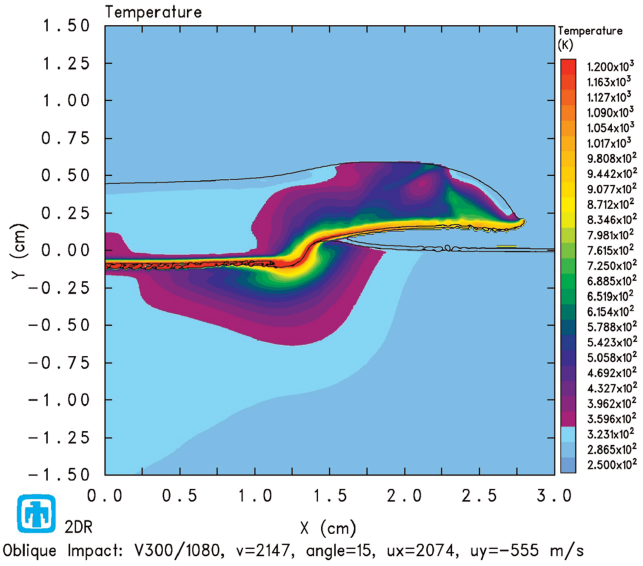

Fig. 15 Temperature profile of test he-1 at 10 μs.

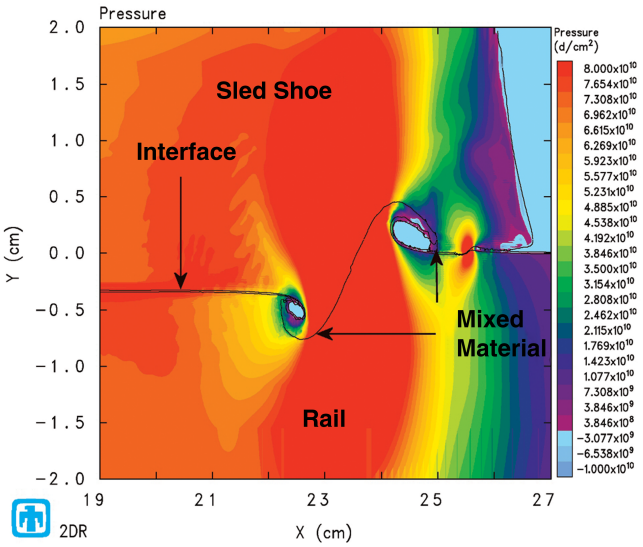

Fig. 18 Typical CTH gouge simulation.

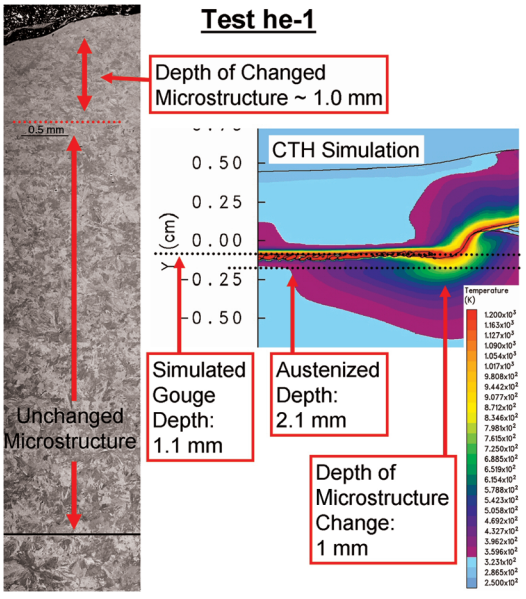

Fig. 16 Comparison of test he-1 at 10 μs.

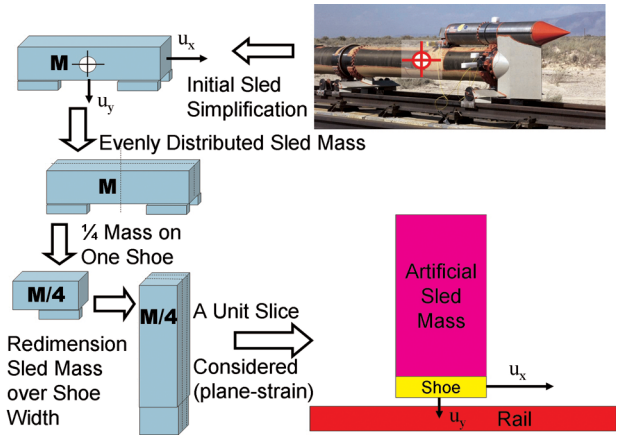

Fig. 17 Development of a plane-strain gouging model [6].

removal, but it does not develop into gouging. This concept of a threshold is analogous to a threshold penetration energy described in previous work [18].

The second kind of impact that creates gouging is simulating shoe contact with a rail discontinuity, rail roughness, or an asperity [4–6]. A collision of the shoe with these kinds of rail conditions causes gouging at the horizontal (downrange) velocities being considered, i.e., 3 km/s. These discontinuities represent actual conditions possible at the HHSTT.

The final type of simulation that can cause gouging is allowing the shoe to strike an angled rail. This would occur in the field when the sled is oscillating during its run and the shoes come down from an oscillation at an angle to the rail. By angling the rail in the simulation, we can replicate the conditions of this collision (i.e., the sled's velocity vector oriented parallel to the shoe). The angle chosen is computed by considering the maximum shoe-gap. This is the designed gap between the rail and the shoe when it is at full travel in the up position, held onto the rail by the bottom arms of the shoe (see Fig. 1b). Allowing this gap on the rear shoe (0.635 cm) creates up to a 0.14 deg angle of incidence at the front shoe, approximately 2.5 m in front of the rear shoe.

Therefore, with these new material models, it is possible to generate gouging by simulating any of these aforementioned conditions. A representative CTH simulated gouge appears in Fig. 18. This particular gouge was created by increasing the vertical kinetic energy to 3 kJ. Below this threshold, the resulting damage to the rail is material deformation and removal, but no material mixing. This type of impact is illustrated in Fig. 19. Note that the rail has experienced deformation, but gouging has not developed. In addition, there is a temperature development through the depth during this kind of nongouging impact.

However, beyond the threshold energy of 3 kJ, gouging would develop, as in Fig. 20. This gouging shows a characteristic mixing of material and a large thermally affected zone, in this case, down to 6 mm below the depth of the gouge.

The other two types of impacts were also investigated by the authors. Hypervelocity gouging was found to occur both in the rail discontinuity case (Fig. 21) and the angled rail impact (Fig. 22). The rail discontinuity was taken to be 0.03048 cm, which matches previous investigations and is a plausible condition on the rail in the field [4–6]. In both of these cases, the vertical impact velocity is 2 m/s and the horizontal velocity is 3 km/s. These impacts generate sufficient energy to initiate the characteristic material mixing that defines gouging.

The investigation of several gouging scenarios found that gouge depth was affected by effective sled mass, which arguably can be allowed to vary between 25 and 100% of the sled mass as we consider an oscillation in which one shoe carries more of the sled mass. That

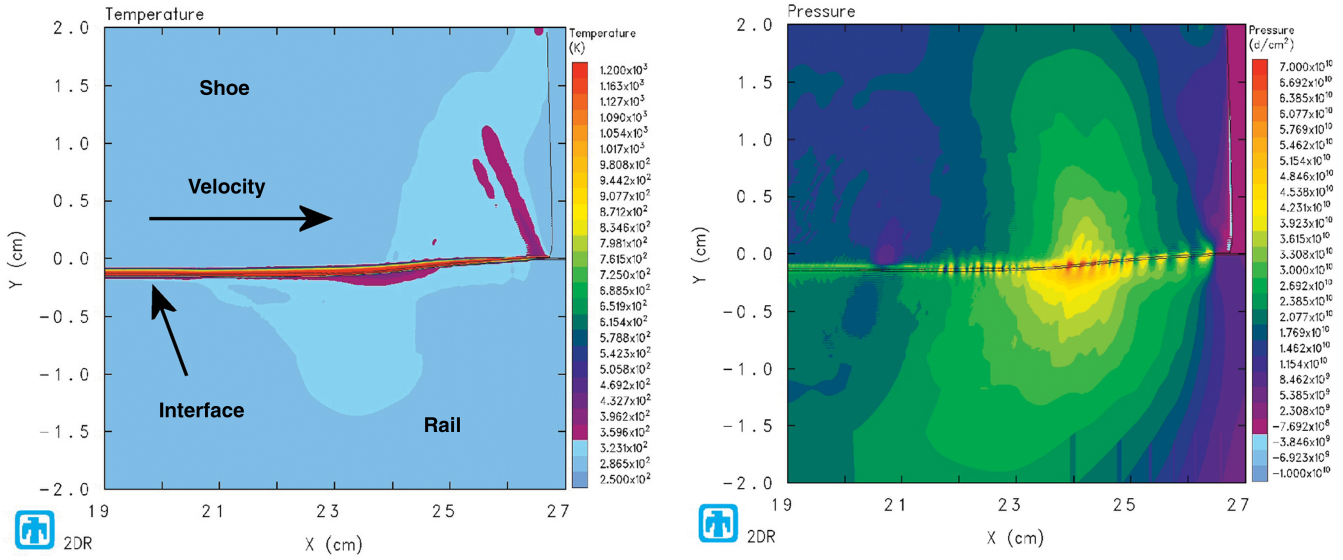

Fig. 19 CTH nongouging simulation, below threshold gouging energy.

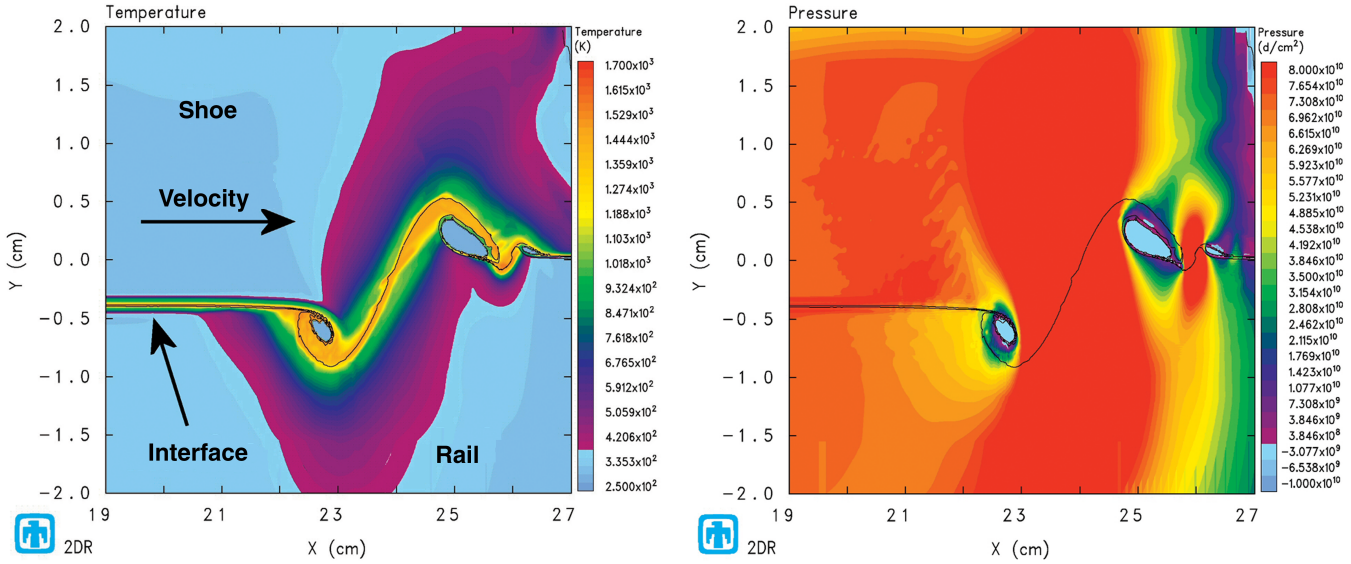

Fig. 20 CTH gouging simulation, above threshold gouging energy.

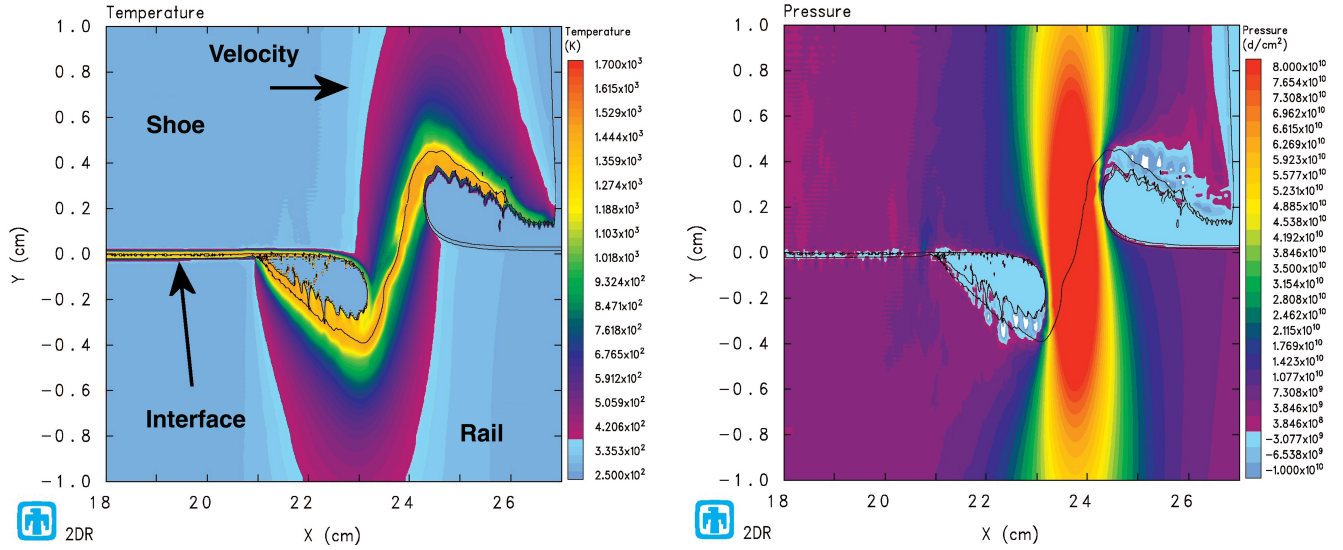

Fig. 21 CTH gouging simulation, rail discontinuity case.

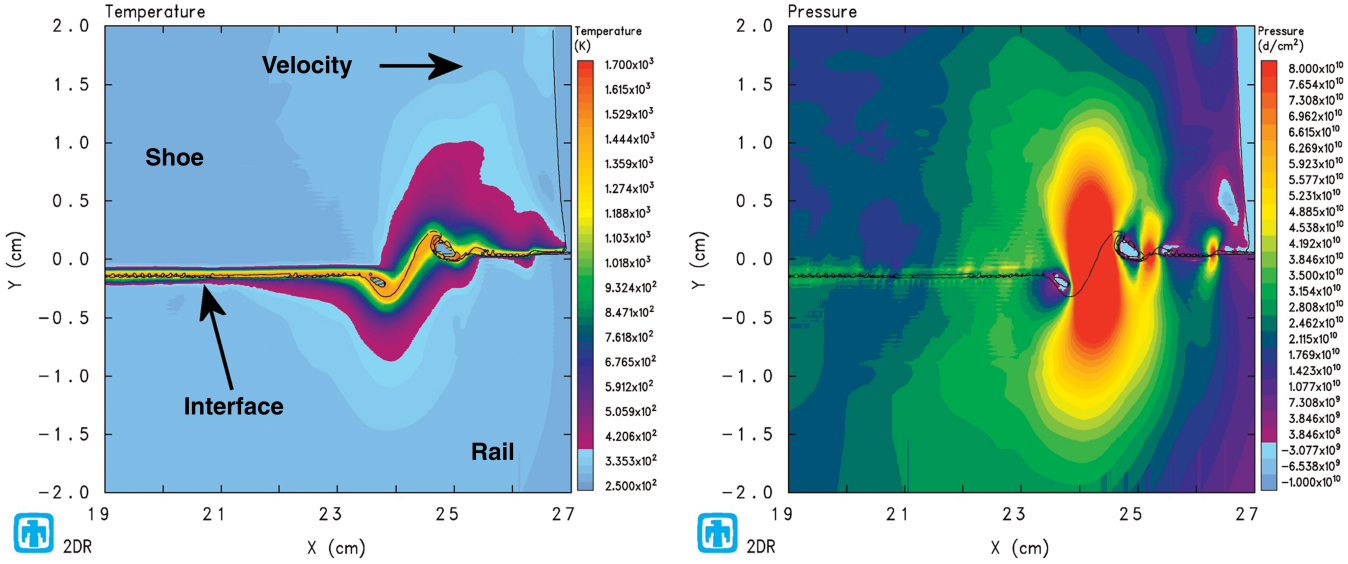

Fig. 22 CTH gouging simulation, angled impact case.

is, as the sled oscillates during a test run, it is plausible that the sled could come back down with more than one-fourth of its mass on one shoe. In the extreme case, all of the mass could be carried by a single shoe.

An important observation that is possible from this CTH simulation of the gouging scenario at the HHSTT is the replication in CTH of the thermal profile necessary to create the microstructure changes reported in the literature [19,20]. The temperatures generated from viscoplastic material deformation are above the austenizing temperatures down to approximately 5 mm below the level of the interface in Figs. 20 and 21. Not only does the amount of material removed in the CTH simulation match the experimentally examined gouge from the HHSTT, but the temperature profile of austenizing down to 5 mm matches exactly also. Therefore, to the extent that we have experimental data, the authors have replicated the experimental gouging, both from the laboratory and from the field, with CTH simulations. These simulations are based on a meticulously formulated material flow model whose foundation is experimental testing and evaluation. Additionally, the final CTH model of the HHSTT scenario promises to allow future investigation into the parameters that lead to gouging and to afford the HHSTT the capability to mitigate those gouging events in the future. For instance, different material choices could be made for the sled shoe, or the shoe/rail impact conditions could be modified to reduce the effects of rail discontinuities.

VI. Conclusions

In this work, new material flow model constants are developed for both VascoMax 300 and 1080 steel from flyer plate impact experiments. The experiments are successfully modeled in CTH, and the Zerilli–Armstrong model is chosen to represent the materials in future modeling due to its capability of matching experimental data across the full range of strain rates.

With these refined material constitutive models, CTH simulations are conducted of experimental impact tests to validate the capability of CTH to replicate observed events. The material models are validated by the excellent agreement achieved between CTH simulations and experimental measurements of the Taylor Impact tests and a series of laboratory hypervelocity gouge tests.

Finally, the refined material models are applied to the HHSTT gouging scenario. The resulting simulations match experimentally examined gouges from the field, and also point to a threshold vertical impact energy required to generate material gouging. Additionally, previously reported gouging results are replicated using rail discontinuities and angled shoe impacts. With the validation of the CTH simulation established, some observations on the conditions necessary to initiate gouging are made. Additionally, the final result of this effort is a full model of the HHSTT gouging scenario, validated against experimental data, which can be used in further studies to mitigate the onset of gouging in hypervelocity tests [22].

Acknowledgments

The authors would like to acknowledge the invaluable support of University of Dayton Research Institute in the performance of the flyer plate experiments. N. S. Brar, Kevin Poorman, and Tim Klopfenstein Jr. made critical contributions in the design, execution, and interpretation of the flyer plate impact experiments. Essential support was also provided by the Air Force Office of Scientific Research (Neal Glassman and John Schmisseur, monitors). Also, Michael Hooser from the Holloman Air Force Base High-Speed Test Track made critical contributions to this endeavor. Additionally, the technical advice of Theodore Nicholas of the Air Force Institute of Technology was instrumental to the research.

References

[1] Gerstle, F. P., Follansbee, P. S., Pearsall, G. W., and Shepard, M. L., "Thermoplastic Shear and Fracture of Steel During High-Velocity Sliding," *Wear*, Vol. 24, No. 1, April 1973, pp. 97–106.

[2] Laird, D. J., and Palazotto, A. N., "Effects of Temperature on the Process of Hypervelocity Gouging," *AIAA Journal*, Vol. 41, No. 11, 2003, pp. 2251–2260.

[3] Laird, D. J., and Palazotto, A. N., "Gouge Development During Hypervelocity Sliding Impact," *International Journal of Impact Engineering*, Vol. 30, No. 2, 2004, pp. 205–223.

[4] Szmerekovsky, A. G., Palazotto, A. N., and Baker, W. P., "Scaling Numerical Models for Hypervelocity Test Sled Slipper-Rail Impacts," *International Journal of Impact Engineering*, Vol. 32, No. 6, 2006, pp. 928–946.

[5] Szmerekovsky, A. G., Palazotto, A. N., and Earnst, M. R., "Numerical Analysis for a Study of the Mitigation of Hypervelocity Gouging," *Proceedings of the 45th AIAA/ASME/ASCE/AHS/ASC Structures, Structural Dynamics, and Materials Conference. Palm Springs, CA, 19–22 April*, AIAA, Reston, VA, 2004, pp. 1–10.

[6] Szmerekovsky, A. G., and Palazotto, A. N., "Structural Dynamic Considerations for a Hydrocode Analysis of Hypervelocity Test Sled Impacts," *AIAA Journal*, Vol. 44, No. 6, 2006, pp. 1–14.

[7] Hertel, E. S., "CTH: a Software Family for Multidimensional Shock Physics Analysis," *Proceedings of the 19th International Symposium on Shock Waves, Marseille, France, 26–30 July*, Vol. 1, Springer–Verlag, New York, 1993, pp. 377–382.

[8] McGlaun, J. M., Thompson, S. L., and Elrick, M. G., "CTH: a Three-Dimensional Shock Wave Physics Code," *International Journal of Impact Engineering*, Vol. 10, Nos. 1–4, 1990, pp. 351–360.

[9] Cinnamon, J. D., Palazotto, A. N., Brar, N. S., Kennan, Z., and Bajaj,

D., "Johnson–Cook Strength Model Constants for VascoMax 300 and 1080 Steels," *Proceedings of the 14th American Physical Society (APS) Topical Conference on Shock Compression of Condensed Matter, Baltimore, MD, 31 July–3 Aug. 2005*, American Physical Society, College Park, MD, Vol. 845, July 2006, pp. 709–712.

[10] Cinnamon, J. D., Palazotto, A. N., and Kennan, Z., "Material Characterization and Development of a Constitutive Relationship for Hypervelocity Impact of 1080 Steel and VascoMax 300," *Proceedings of the 2005 Hypervelocity Impact Symposium, Lake Tahoe, CA, 10–14 Oct. 2005*, *International Journal of Impact Engineering*, Vol. 33, Nos. 1–12, Dec. 2006, pp. 180–189.

[11] Cinnamon, J. D., and Palazotto, A. N., "Refinement of a Hypervelocity Model for the Rocket Sled Test," *Proceedings of the 2005 American Society of Mechanical Engineers (ASME) International Mechanical Engineering Congress and Exposition, Orlando, FL, 5–11 Nov.*, American Society of Mechanical Engineers, New York, 2005, pp. 1–10; also American Society of Mechanical Engineers Paper IMECE2005-80004, 2005.

[12] Yun, S., Cinnamon, J. D., and Palazotto, A. N., "Further Refinement and Validation of a Viscoplastic Model for VascoMax 300 and 1080 Steel Considering Plastic Deformation Characterization," *Mechanics of Materials* (submitted for publication), Reed–Elsevier, New York, 2006.

[13] Johnson, G. R., and Cook, W. H., "Constitutive Model and Data for Metals Subjected to Large Strains, High Strain Rates, and High Temperatures," *Proceedings of the 7th International Symposium Ballistics*, American Defense Preparation Organization, Hague, The Netherlands, April 1983, pp. 541–547.

[14] Zerilli, F. J., and Armstrong, R. W., "Dislocation-Mechanics-Based Constitutive Relations for Material Dynamics Calculations," *Journal of Applied Physics*, Vol. 61, No. 5, March 1987, pp. 1816–1825.

[15] Nicholas, T., Rajendran, A. M., and Grove, D. J., "Analytical Modeling of Precursor Decay in Strain-Rate Dependent Materials," *International Journal of Solids and Structures*, Vol. 23, No. 12, 1987, pp. 1601–1614.

[16] Nicholas, T., Rajendran, A. M., and Grove, D. J., "Offset Yield Criterion for Precursor Decay Analysis," *Acta Mechanica*, Vol. 69, Nos. 1–4, Dec. 1987, pp. 205–218.

[17] Cinnamon, J. D., Palazotto, A. N., Szmerekovsky, A. G., and Pendleton, R. J., "Further Investigation of a Scaled Hypervelocity Gouging Model and Validation of Material Constitutive Models," *47th AIAA/ASME/ASCE/AHS/ASC Structures, Structural Dynamics, and Materials Conference, Newport, RI, 1–4 May*, AIAA, Reston, VA, 2006, pp. 1–20.

[18] Cinnamon, J. D., and Palazotto, A. N., "Further Validation of a General Approximation for Impact Penetration Depth Considering Hypervelocity Gouging Data," *International Journal of Impact Engineering*, Vol. 34, No. 8, Aug. 2007, pp. 1307–1326.

[19] Cinnamon, J. D., and Palazotto, A. N., "Metallographic Examination of Thermal Effects in Hypervelocity Gouging," *Proceedings of the 2005 American Society of Mechanical Engineers (ASME) Pressure Vessel and Piping Conference, Denver, CO, 17–21 July*, American Society of Mechanical Engineers, New York, 2005, pp. 1–9; also American Society of Mechanical Engineers Paper PVP2005-71613, 2005.

[20] Cinnamon, J. D., and Palazotto, A. N., "Metallographic Examination and Validation of Thermal Effects in Hypervelocity Gouging," *ASME Journal of Pressure Vessel Technology*, Vol. 129, No. 1, Feb. 2007, pp. 133–141.

[21] Cinnamon, J. D., Palazotto, A. N., Szmerekovsky, A. G., and Pendleton, R. J., "Investigation of a Scaled Hypervelocity Gouging Model and Validation of Material Constitutive Models," *AIAA Journal* Vol. 45, No. 5, 2007 .

[22] Cinnamon, J. D., "Analysis and Simulation of Hypervelocity Gouging Impacts," Ph.D. Dissertation, Air Force Inst. of Technology, AFIT/DS/ENY/06-01, June 2006, pp. 1–312.

T. Nicholas
Associate Editor